ADVANCED MATERIALS
www.advmat.de

Polymers with Side Chain Porosity for Ultrapermeable and Plasticization Resistant Materials for Gas Separations

*Yuan He, Francesco M. Benedetti, Sharon Lin, Chao Liu, Yanchuan Zhao, Hong-Zhou Ye, Troy Van Voorhis, M. Grazia De Angelis, Timothy M. Swager, and Zachary P. Smith**

Polymer membranes with ultrahigh CO_2 permeabilities and high selectivities are needed to address some of the critical separation challenges related to energy and the environment, especially in natural gas purification and post-combustion carbon capture. However, very few solution-processable, linear polymers are known today that access these types of characteristics, and all of the known structures achieve their separation performance through the design of rigid backbone chemistries that concomitantly increase chain stiffness and interchain spacing, thereby resulting in ultramicroporosity in solid-state chain-entangled films. Herein, the separation performance of a porous polymer obtained via ring-opening metathesis polymerization is reported, which possesses a flexible backbone with rigid, fluorinated side chains. This polymer exhibits ultrahigh CO_2 permeability (>21 000 Barrer) and exceptional plasticization resistance (CO_2 plasticization pressure > 51 bar). Compared to traditional polymers of intrinsic microporosity, the rate of physical aging is slower, especially for gases with small effective diameters (i.e., He, H_2, and O_2). This structural design strategy, coupled with studies on fluorination, demonstrates a generalizable approach to create new polymers with flexible backbones and pore-forming side chains that have unexplored promise for small-molecule separations.

Y. He, H.-Z. Ye, Prof. T. Van Voorhis, Prof. T. M. Swager
Department of Chemistry
Massachusetts Institute of Technology
Cambridge, MA 02139, USA

F. M. Benedetti, S. Lin, Prof. Z. P. Smith
Department of Chemical Engineering
Massachusetts Institute of Technology
Cambridge, MA 02139, USA
E-mail: zpsmith@mit.edu

F. M. Benedetti, Prof. M. G. De Angelis
Department of Civil, Chemical, Environmental, and Materials Engineering
University of Bologna
40131 Bologna, Italy

Dr. C. Liu, Prof. Y. Zhao
Key Laboratory for Organofluorine Chemistry
Center for Excellence in Molecular Synthesis
Shanghai Institute of Organic Chemistry
University of Chinese Academy of Sciences
Chinese Academy of Sciences
345 Ling-Ling Road, Shanghai 200032, China

The ORCID identification number(s) for the author(s) of this article can be found under https://doi.org/10.1002/adma.201807871.

DOI: 10.1002/adma.201807871

Membranes are a promising platform technology for energy-efficient chemical separations. Unlike other separation processes, membranes do not require thermal regeneration, phase changes, or moving parts.[1] Increasing the permeability of polymer membranes used for gas separations is essential for enhancing productivity and reducing membrane areas required for large-scale gas and vapor separations.[2] Specific membrane applications include natural gas purification, hydrogen separations, air separation, and CO_2 capture from flue gas.[3,4]

Over the past decade, polymers of intrinsic microporosity (PIMs) have defined the state-of-the-art for gas separations.[5,6] Their rigid and contorted backbone structures lead to excellent separation performance for a variety of challenging binary separations (e.g., CO_2/N_2, CO_2/CH_4, O_2/N_2, and H_2/CH_4).[5] Guided by the discovery that polymers of intrinsic miroporosity[7] now called PIMs were highly effective for gas separation,[8] researchers have sought to extend the database of accessible structures by designing and synthesizing ladder-type porous polymers containing more rigid backbones with even less conformational freedom.[9,10] Despite the advances in backbone rigidity of polymer chains, a relatively unexplored design strategy of creating porous polymers is to attach rigid, free-volume-generating side chains to a flexible backbone to form a type of "bottlebrush" polymer. Recently, some of us have found that these polymers can be highly porous as a result of inefficient packing between rigid, noncompliant side chains.[11] In addition, since rigid macromonomers containing polymerizable units are synthesized before polymerization (**Scheme 1**a), it is easier to incorporate a variety of unique and predesigned functionalities into this class of polymer as compared to PIM-1, which mainly relies on post-polymerization functionalization.[12,13] From a transport perspective, predesigning side chain structures can enhance the morphological ordering of ultramicropores, enabling easier access to controlled entropic selectivities that are not currently considered from the activated state theory approach used to define the current polymer upper bound.[14]

It is well-known that fluorinated polymers introduce properties such as thermal stability and nonwettability, which

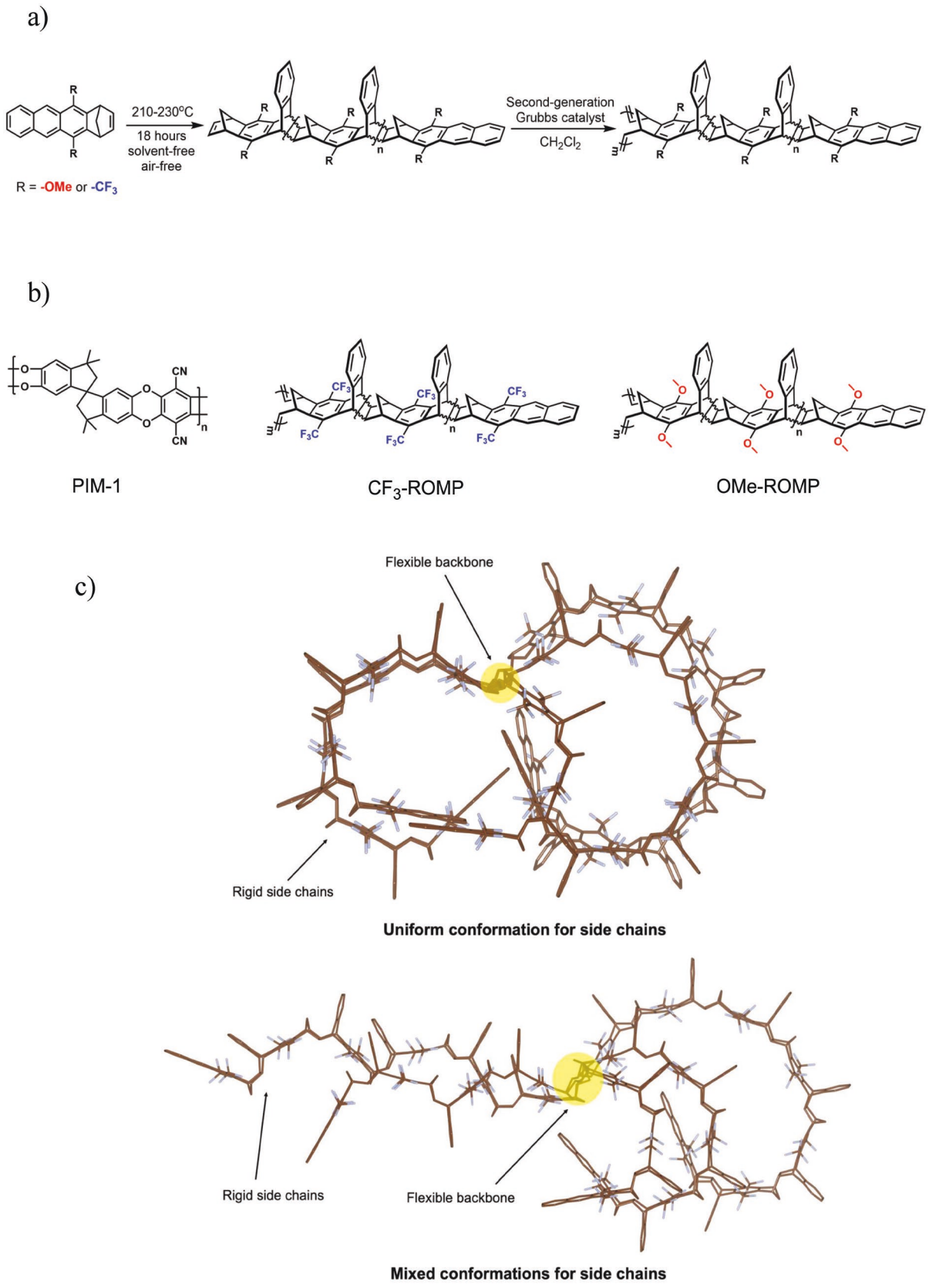

Scheme 1. a) Generalized synthetic procedure for CF_3-ROMP and OMe-ROMP. b) Molecular structures of PIM-1, CF_3-ROMP, and OMe-ROMP. c) Schematic representation of CF_3-ROMP with five repeating units (uniform conformation or mixed conformations for side chains).

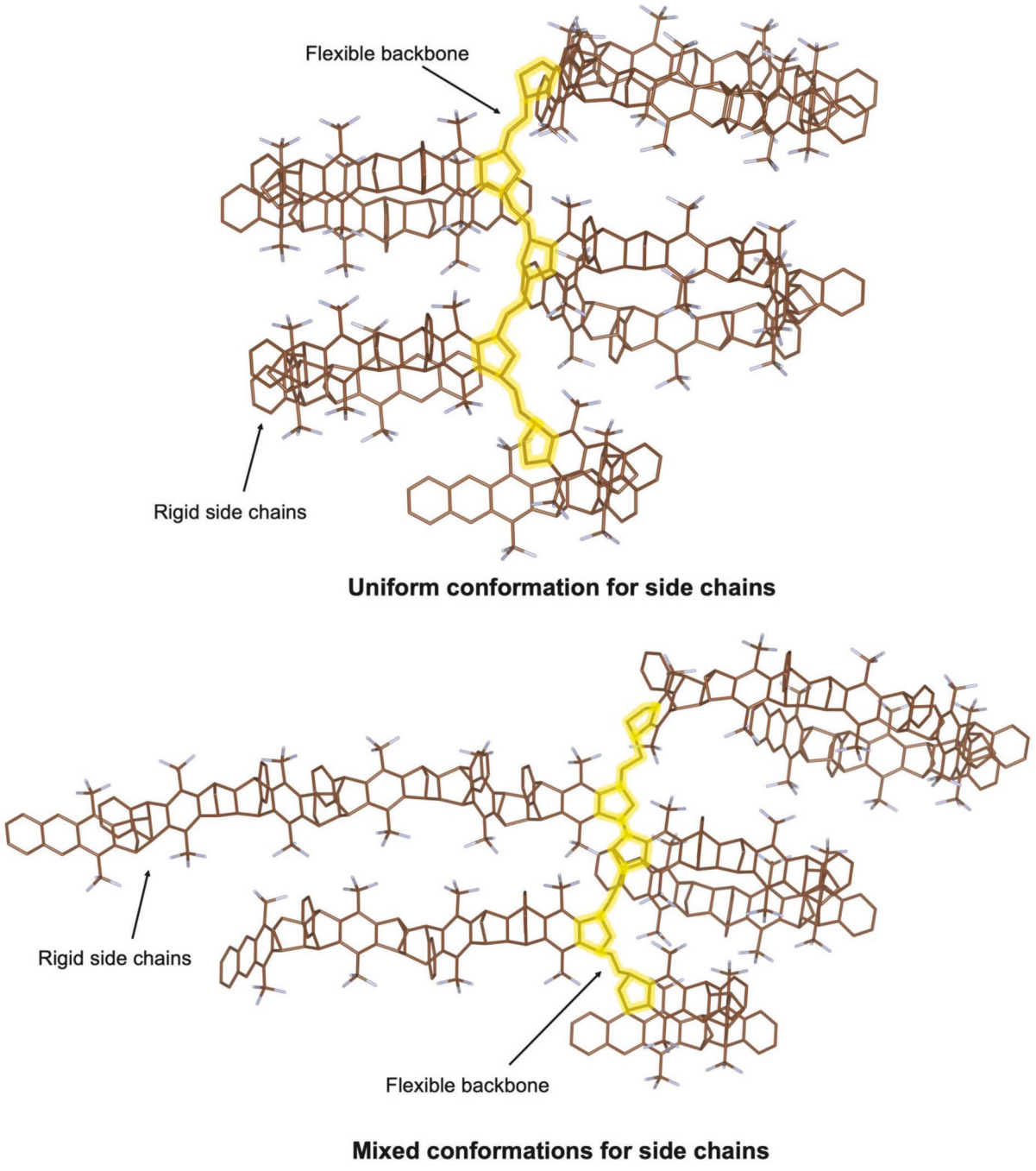

Scheme 1. Continued.

have enabled commercial applications.[15] In terms of gas separation, previous studies have shown that the introduction of fluorinated moieties in aromatic polyimides can dramatically increase gas permeability with little impact on permselectivity.[16] In poly(organosiloxanes), it was found that CO_2 permeability and CO_2/CH_4 selectivity could increase simultaneously by incorporating fluorine-containing groups.[17] In all these cases, bulky hexafluoroisopropylidene functionality is used to contort the polymer backbone and generate free volume, thereby enhancing separation performance. Considering the synthetic versatility of using pore-forming macromonomers, the approach presented here enables a systematic comparison for studying the effect of fluorination on gas transport properties relative to that of hydrocarbon analogs in predesigned ultramicropores. By doing so, a more direct deconvolution of the morphological and electronic contributions of fluorinated functionality on gas transport can be achieved.

Here, we describe the gas transport properties of two porous polymers obtained via ring-opening metathesis polymerization (ROMP), which both possess flexible poly(norbornene)

backbones with rigid side chains. Films of CF_3-ROMP exhibited ultrahigh CO_2 permeability (>21 000 Barrer) and exceptional plasticization resistance (CO_2 plasticization pressure > 51 bar). The structures of two porous ROMP polymers are shown in Scheme 1b and are based on synthetic procedures published previously.[11] Side chains are made via an iterative Diels–Alder reaction, which generates a mixture of oligomers with different chain lengths (typically with 2–9 repeating units) (Figures S1 and S2, Supporting Information). The mixture of oligomers is directly used for ROMP polymerization. Schematic representations of CF_3-ROMP are shown in Scheme 1c. Both CF_3-ROMP and OMe-ROMP are readily soluble in common organic solvents, allowing characterization by NMR and GPC (Figures S3 and S4, Supporting Information). The precast CF_3-ROMP and OMe-ROMP powder showed significant microporosity via N_2 adsorption isotherms at 77 K, with a Brunauer–Emmett–Teller (BET) surface area of 700 and 146 $m^2\ g^{-1}$, respectively (Figure S6, Supporting Information). Solution casting from chloroform led to optically clear films (Figure S9, Supporting Information) suitable for gas permeation studies.

The gas separation performance of CF_3-ROMP, OMe-ROMP, and PIM-1 are shown in **Figure 1** and Table S1 (Supporting Information). Before permeation experiments, films were first soaked in ethanol for 48 h, dried at ambient conditions for 24 h, and then degassed in full vacuum for 8 h at 35 °C to remove residual solvent, as confirmed by thermal gravimetric analysis (TGA) (Figure S10, Supporting Information).[18] The effect of different treatment conditions and film history were also investigated (Section 7, Supporting Information). The magnitude of gas permeability for CF_3-ROMP and OMe-ROMP followed the order of $CO_2 > H_2 > O_2 > He > CH_4 > N_2$, indicating a strong solubility contribution to permeation (Figure S11a, Supporting Information). CF_3-ROMP exhibited exceptionally high gas permeabilities across all gases tested, notably for CO_2 (≈21 300 Barrer) and H_2 (≈8300 Barrer) for the non-aged film. These gas permeabilities were about 60% to 200% higher than the non-aged PIM-1 film under the same ethanol treatment and testing conditions, which makes CF_3-ROMP the third most permeable linear ultramicroporous polymer reported to date, behind PTMSP and PIM-TMN-Trip reported by Rose et al.[9] As a result, CF_3-ROMP surpassed the 2008 Robeson upper bound for H_2/CH_4 after physical aging, and was above the

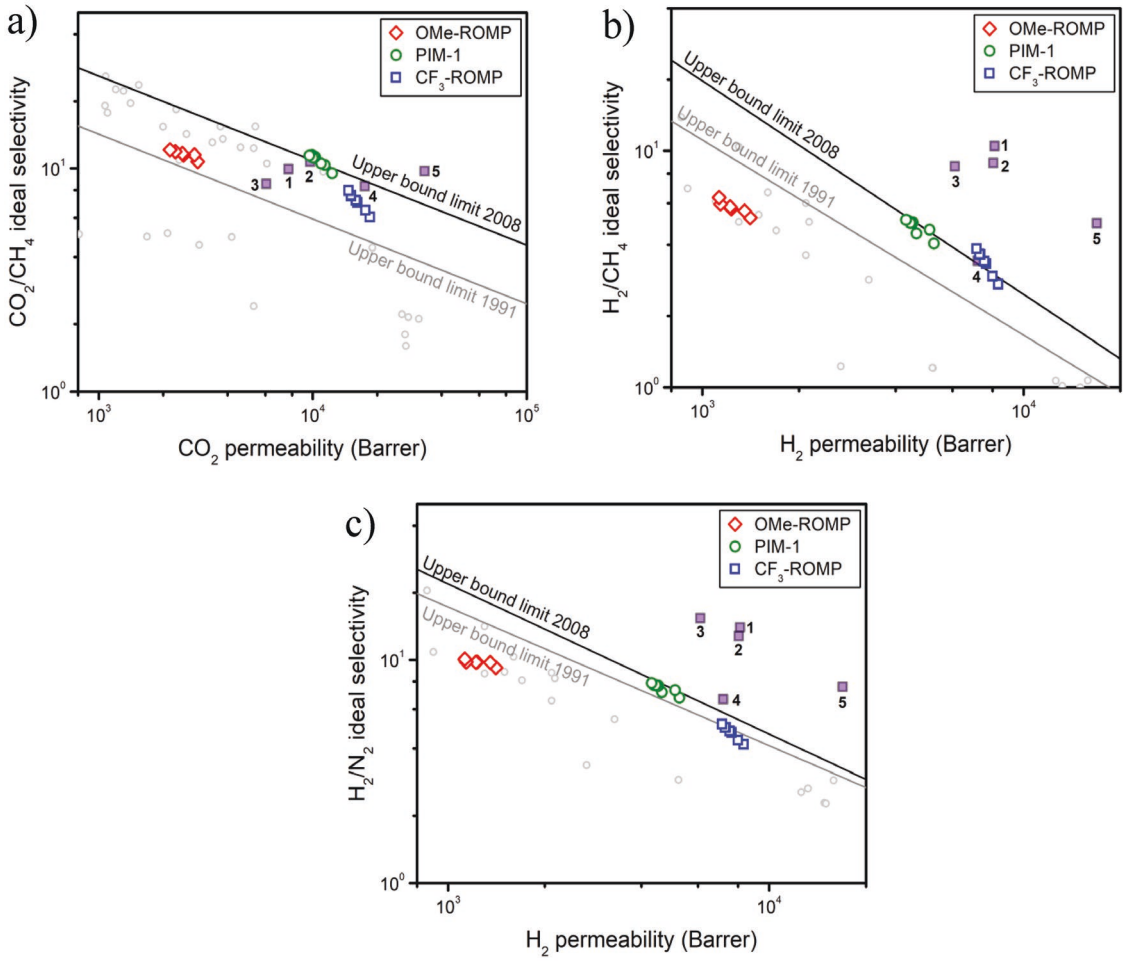

Figure 1. a–c) Robeson plots of CF_3-ROMP, OMe-ROMP, and PIM-1 for CO_2/CH_4 (a), H_2/CH_4 (b), H_2/N_2 (c) gas pairs as a function of physical aging time. The black and gray lines represent 2008 and 1991 upper bounds, respectively.[23,24] The filled purple squares represent other highly permeable PIMs reported: 1) PIM-EA-TB, 2) PIM-Trip-TB, 3) PIM-TMN-SBI, 4) PIM-TMN-Trip-TB, 5) PIM-TMN-Trip.[9,25]

1991 Robeson upper bound for all other gas pairs investigated (Figure 1; Figure S12, Supporting Information).

In contrast, OMe-ROMP exhibited significantly lower gas permeabilities compared to CF_3-ROMP and PIM-1 but higher permselectivities (Figure 1; Figure S11d, Supporting Information). These striking differences in transport properties are notable because CF_3-ROMP and OMe-ROMP are structurally very similar with the main exception being the $–CF_3$ versus –OMe functionality. Quantitatively, gas permeabilities are seven to ten fold higher, depending on the gas, for the CF_3-ROMP. This difference in performance can be rationalized by the higher BET surface area of CF_3-ROMP arising from the random configuration of CF_3- and OMe-substituted side chains. The pendant $–CF_3$ group is bulkier and stiffer than –OMe, which hinders interchain packing and reduces intrachain rotational freedom, thus leading to higher porosity. Fluorine-containing moieties are also known to have high solubilities for light gases, which could subsequently increase permeabilities in the framework of the solution-diffusion model.[19–21] It may be the combination of these two effects that leads to the significant increase in gas permeabilities, similar to trends reported for certain polyimides and polycarbonates.[22] Molecular mechanics simulations suggest side chain bending into "pocket-shapes" are a potentially pseudo-stable conformation (Section 4, Supporting Information). We also hypothesize that the pendant $–CF_3$ groups may form localized fluorine-rich domains between side chain segments as a result of the curvature of the side chain in 3D (Scheme 1c). However, the stereochemistry of Diels–Alder reaction during side chain formation is disordered and hence there is a distribution of the shape and size of the pockets.

Compared to PIM-1, CF_3-ROMP exhibited moderately lower selectivities for the gas pairs CO_2/CH_4, H_2/CH_4, and H_2/N_2. Diffusivity-selectivity and solubility-selectivity is presented in Figures S19 and S21 in the Supporting Information. According to **Figure 2**, Figures S13 and S14 (Supporting Information), the solubility-selectivity of CF_3-ROMP is close to that of PIM-1 whereas its diffusivity-selectivity is lower for the majority of gas pairs. Considering the difference in pore-size distribution between two polymers (Figure S6, Supporting Information), we hypothesize that the lower diffusivity-selectivity of CF_3-ROMP is most likely caused by polydispersity in length and stereochemistry of the side chains. Given this hypothesis, diffusivity-selectivity may be improved by homogenizing the length of side chains and devising systems that do not have structural variances as a result of the stereochemistry of the Diels–Alder reaction used in the side chain synthesis.

In addition to evaluating performance relative to the upper bounds, determining the effects of penetrant-induced plasticization is an important concern in membrane-based gas separations.[26] Exposure of membranes to strongly interacting gases such as CO_2 at high pressures can reduce permselectivity as a result of sorption-induced swelling.[27] Thus, membranes that maintain stable performance under high CO_2 feed pressures are desirable. In **Figure 3**a, CF_3-ROMP, OMe-ROMP, and PIM-1 were subjected to CO_2 feed pressure up to 51 bar. Of note, CO_2 permeabilities of CF_3-ROMP decreased monotonically up to 51 bar even when using fugacity to account for nonidealities (Figure S25, Supporting Information). This result reveals that the plasticization pressure point, above which permeability starts to increase, was not reached under the conditions considered for these experiments. PIMs and many other non-crosslinked porous polymers exhibit plasticization pressure points at significantly lower pressures (Figures S23 and Table S2, Supporting Information), but the non-crosslinked CF_3-ROMP and OMe-ROMP have plasticization pressure points more characteristic to those of chemically-crosslinked polyimides.[28,29] Moreover, when the CO_2 feed pressure was gradually decreased, the hysteresis induced by conditioning up to 51 bar was ≈35% of the original CO_2 permeability. OMe-ROMP shows similar antiplasticization behavior with plasticization pressure points >51 bar, but the hysteresis (≈50%) is slightly higher than CF_3-ROMP. As a comparison, the plasticization pressure point for PIM-1 when tested under identical conditions was ≈27 bar, and it shows a significantly larger hysteresis effect (up to 95% increased permeability) when CO_2 feed pressure is released. These results indicate that the interchain cohesive energy for ROMPs is larger than that of PIM-1. This feature may originate from both a fluorophilic interaction

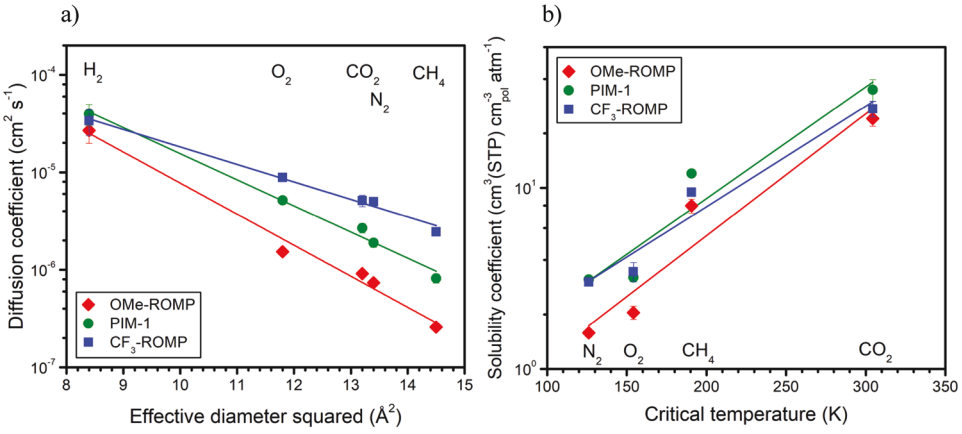

Figure 2. a) Diffusion coefficient plotted against effective diameter squared for CF_3-ROMP, OMe-ROMP, and PIM-1 at 1 h aging after liquid ethanol soaking for 48 h, air-drying for 24 h, and subjecting to full vacuum for 8 h at 35 °C. The steepness of the slope indicates molecular sieving capabilities, thus molecular sieving capabilities decrease in the following order: –OMe > PIM-1 > $–CF_3$. b) Solubility coefficient of N_2, O_2, CH_4, and CO_2 in polymers as a function of critical temperature.

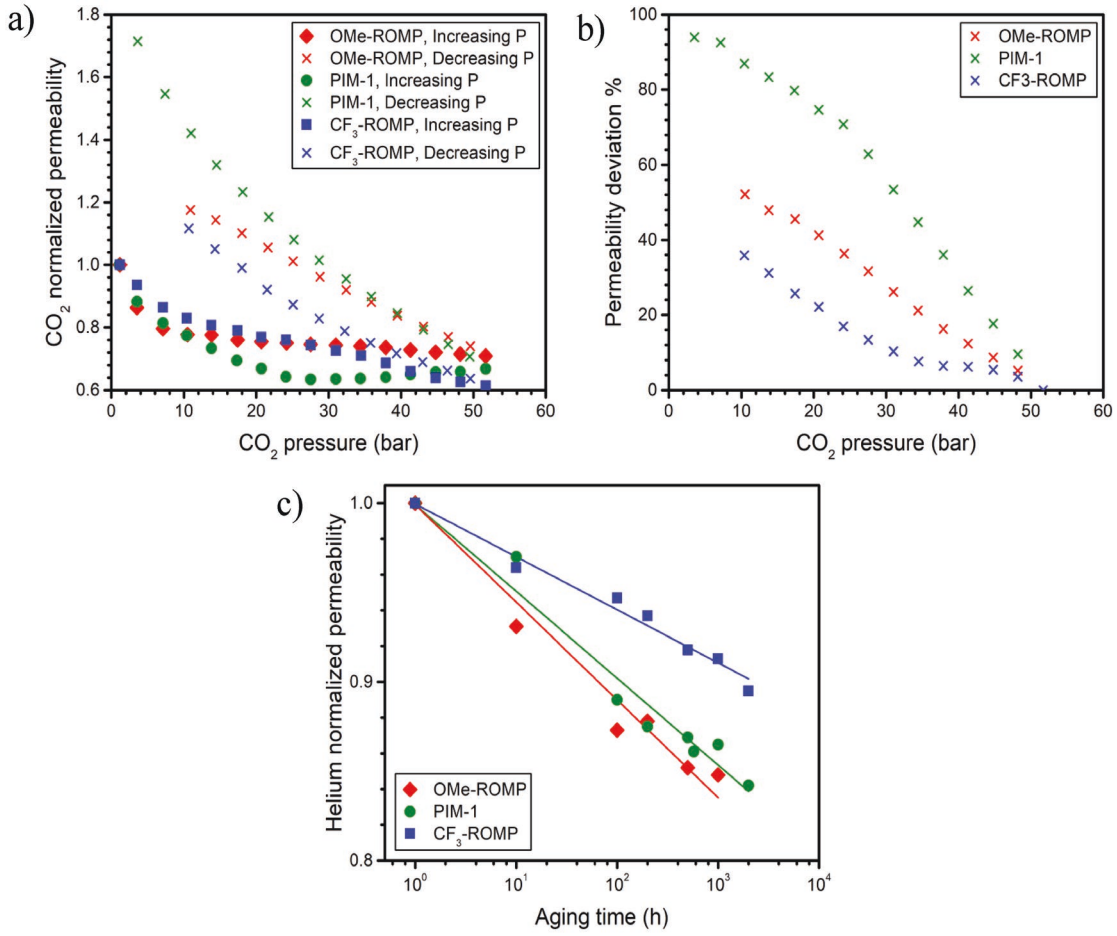

Figure 3. a) CO_2 plasticization study and b) hysteresis induced by conditioning of the film at 51 bar of CO_2 for CF_3-ROMP, OMe-ROMP, and PIM-1. c) Physical aging study of helium by monitoring permeability over time for CF_3-ROMP, OMe-ROMP, and PIM-1 between 1 and 2000 h after liquid ethanol treatment.

between $-CF_3$ moieties and a greater rigidity-promoting "physical interlocking" between side chains typical of both ROMPs. Such an interpretation is in agreement with the results of Swaidan et al., wherein interchain rigidity contributed to CO_2 plasticization resistance.[12,30] To further investigate the plasticization resistance of CF_3-ROMP, 50:50 vol% CO_2/CH_4 mixed-gas permeation experiments were run, and the details can be found in Section 11 of the Supporting Information.

It is well-known that the relaxation of non-equilibrium free volume elements in PIMs proceeds rapidly in the first ≈10 d after swelling in a nonsolvent (e.g., alcohols).[31] To evaluate such behavior in the samples considered here, physical aging of CF_3-ROMP, OMe-ROMP, and PIM-1 was monitored by gas permeation measurements and wide-angle X-ray scattering (WAXS) for 2000 h. Figure 3b displays helium permeability as a function of the time, and it is clear that CF_3-ROMP, OMe-ROMP, and PIM-1 age at different rates. For smaller gases like He, H_2, and O_2, CF_3-ROMP aged the slowest among samples considered, while OMe-ROMP aged the fastest with PIM-1 displaying intermediate behavior (Figure S17, Supporting Information). Notably, the aging rate of CF_3-ROMP is significantly lower than that of state-of-the-art PIMs, although the alcohol treatment was slight different (ethanol vs methanol).[9,32] For instance, helium permeability decreased by ≈45% after 1000 h aging for PIM-TMN-Trip, whereas CF_3-ROMP only decreased by ≈10%. Moreover, the CF_3-ROMP films considered here are thinner than PIM-TMN-Trip (119 vs 192 μm), and physical aging is accelerated for thinner films.[33] For larger molecules like CO_2, N_2, and CH_4, there was no significant difference in aging rates between the three polymers compared in this work (Figure S17a, Supporting Information). These findings suggest that using permeability as a proxy for assessing aging rates instead of diffusion is a limitation for more strongly sorbing components that also have significant solubility contributions to permeability.

Previous studies have shown that the introduction of fluorinated moieties can suppress physical aging in aromatic polyimides.[34,35] In the case at hand, despite its higher BET surface area, the aging rate of CF_3-ROMP was considerably lower than that of OMe-ROMP for gases with smaller effective diameters. The WAXS of CF_3-ROMP displays a decrease in scattering intensity only over the larger *d*-spacing regime during physical aging, whereas OMe-ROMP exhibited a decrease in scattering intensity across the entire *d*-spacing range (Figure S22,

Supporting Information). This trend suggests that subtle differences in polymer chemistry for a similar polymer design may result in multiple, complex aging pathways. The reduced aging rate for CF_3-ROMP compared to OMe-ROMP likely results from a stability of CF_3-ROMP to contraction of smaller free volume elements (Figures S15 and S16, Supporting Information).

In summary, we have demonstrated a versatile approach to achieve ultrahigh CO_2 permeabilities and selective size-sieving behavior for gas-phase separations by using pore-forming side chains attached to flexible polymer backbones. Pendent $–CF_3$ groups enhance gas permeability and reduce physical aging compared to their –OMe counterparts. The different performance metrics as a function of pendent groups on the side chain reveal that these features can be used to tailor gas separation performance. Outstanding plasticization resistance is a common feature for both of the ROMP polymers presented, indicating that this new structural design may provide a material platform to systematically address challenges with plasticization. Moreover, CF_3-ROMP exhibited a reduction in physical aging rate compared to PIM-1 even though it is characterized by significantly higher intrinsic permeabilities. The formation of porous polymers based on flexible backbones and rigid free volume promoting side chains represents a promising new platform of materials for addressing fundamental limitations in current design strategies for membrane materials.

Experimental Section

Synthesis of Porous ROMP Polymers: Synthetic procedures for CF_3-ROMP and OMe-ROMP have been previously reported by Zhao et al.[11]

Modeling and Gas Transport Properties: The 3D structure of CF_3-ROMP is optimized using the MMFF 94 force field as implemented in Avogadro 1.2.0.

Gas Transport Properties: Self-standing films of CF_3-ROMP, OMe-ROMP, and PIM-1 were prepared by slow evaporation of a 3 wt% polymer solution in chloroform using a flat aluminum Petri dish. The as-cast film was soaked in liquid ethanol before testing gas permeability and WAXS. TGA analysis was performed to ensure the complete removal of residual solvents from the films and to determine their thermal stability. The thicknesses of CF_3-ROMP, OMe-ROMP, and PIM-1 films, as measured with a digital micrometer, were 119, 160, and 119 µm, respectively. Permeability was measured at 35 °C with a fixed-volume variable-pressure Maxwell Robotics automated permeation system from the slope of the curve (p, t) in the steady-state region after six times the time lag (θ). Pressure was measured with a MKS transducer (Model 622C, 10 Torr limit). The diffusion coefficient, $\mathcal{D}$, was determined by applying the time-lag method: $\mathcal{D} = l^2/6\theta$ where l is the film thickness. The solubility coefficient, $\mathcal{S}$, was determined in the framework of the solution-diffusion model where $\mathcal{S} = \frac{\mathcal{P}}{\mathcal{D}}$ Aging experiments were systematically performed on samples subjected to the same treatment and storage conditions, experiencing the same history for up to 2000 h. CO_2-induced plasticization experiments were performed by pressurizing samples up to 51 bar and depressurizing down to 1 bar to evaluate the hysteresis.

Supporting Information

Supporting Information is available from the Wiley Online Library or from the author.

Acknowledgements

Y.H. and F.M.B. contributed equally to this work. The authors declare the following competing financial interest(s): a patent has been filed on the polymers reported in this paper and their gas separation applications. F.M.B. acknowledges the Marco Polo Scholarship by Department of Civil, Chemical, Environmental and Materials Engineering, Alma Mater Studiorum, University of Bologna. The authors are grateful to Ashleigh L. Ward, Stephen M. Meckler, Mark Carrington, and Brett A. Helms for providing PIM-1 sample used in this work. Work at the Molecular Foundry, including PIM-1 synthesis and characterization, was supported by the Office of Science, Office of Basic Energy Sciences, of the U.S. Department of Energy under Contract No. DE-AC02-05CH11231. The authors are grateful to Prof. Haiqing Lin and Liang Huang at the University of Buffalo for assisting with mixed-gas experiments. This work is supported by National Science Foundation through award DMR-1410718. Transport characterization work by S.L. is supported in part by the U.S. Department of Energy, Office of Science, Office of Basic Energy Sciences, Separation Science program under Award Number DE-SC0019087.

Conflict of Interest

The authors declare the following competing financial interest(s): a patent has been filed on the polymers reported in this paper and their gas separation applications.

Keywords

backbone flexibility, gas separation, porous polymers, ROMP, side chain rigidity

Received: December 5, 2018
Revised: March 7, 2019
Published online: April 9, 2019

[1] M. Galizia, W. S. Chi, Z. P. Smith, T. C. Merkel, R. W. Baker, B. D. Freeman, *Macromolecules* **2017**, *50*, 7809.
[2] Y. Yampolskii, *Macromolecules* **2012**, *45*, 3298.
[3] C. G. Bezzu, M. Carta, A. Tonkins, J. C. Jansen, P. Bernardo, F. Bazzarelli, N. B. Mckeown, *Adv. Mater.* **2012**, *24*, 5930.
[4] S. Wang, X. Li, H. Wu, Z. Tian, Q. Xin, G. He, D. Peng, S. Chen, Y. Yin, Z. Jiang, M. D. Guiver, *Energy Environ. Sci.* **2016**, *9*, 1863.
[5] N. B. McKeown, P. M. Budd, *Chem. Soc. Rev.* **2006**, *35*, 675.
[6] Z. X. Low, P. M. Budd, N. B. McKeown, D. A. Patterson, *Chem. Rev.* **2018**, *118*, 5871.
[7] T. M. Long, T. M. Swager, *J. Am. Chem. Soc.* **2003**, *125*, 14113.
[8] P. M. Budd, B. S. Ghanem, S. Makhseed, N. B. McKeown, K. J. Msayib, C. E. Tattershall, *Chem. Commun.* **2004**, *4*, 230.
[9] I. Rose, C. G. Bezzu, M. Carta, B. Comesanã-Gándara, E. Lasseuguette, M. C. Ferrari, P. Bernardo, G. Clarizia, A. Fuoco, J. C. Jansen, K. E. Hart, T. P. Liyana-Arachchi, C. M. Colina, N. B. McKeown, *Nat. Mater.* **2017**, *16*, 932.
[10] S. Liu, Z. Jin, Y. C. Teo, Y. Xia, *J. Am. Chem. Soc.* **2014**, *136*, 17434.
[11] Y. Zhao, Y. He, T. M. Swager, *ACS Macro Lett.* **2018**, *7*, 300.
[12] R. Swaidan, B. Ghanem, M. Al-Saeedi, E. Litwiller, I. Pinnau, *Macromolecules* **2014**, *47*, 7453.
[13] N. Du, H. B. Park, G. P. Robertson, M. M. Dal-Cin, T. Visser, L. Scoles, M. D. Guiver, *Nat. Mater.* **2011**, *10*, 372.
[14] B. D. Freeman, *Macromolecules* **1999**, *32*, 375.
[15] M. G. Dhara, S. Banerjee, *Prog. Polym. Sci.* **2010**, *35*, 1022.

[16] J. R. Wiegand, Z. P. Smith, Q. Liu, C. T. Patterson, B. D. Freeman, R. Guo, *J. Mater. Chem. A* **2014**, *2*, 13309.
[17] S. Alexander Stern, *J. Membr. Sci.* **1994**, *94*, 1.
[18] C. R. Mason, L. Maynard-Atem, N. M. Al-Harbi, P. M. Budd, P. Bernardo, F. Bazzarelli, G. Clarizia, J. C. Jansen, *Macromolecules* **2011**, *44*, 6471.
[19] M. F. Costa Gomes, A. A. H. Pádua, *J. Phys. Chem. B* **2003**, *107*, 14020.
[20] D. F. Sanders, Z. P. Smith, R. Guo, L. M. Robeson, J. E. McGrath, D. R. Paul, B. D. Freeman, *Polymer* **2013**, *54*, 4729.
[21] J. G. Wijmans, R. W. Baker, *J. Membr. Sci.* **1995**, *107*, 1.
[22] M. W. Hellums, W. J. Koros, G. R. Husk, D. R. Paul, *J. Membr. Sci.* **1989**, *46*, 93.
[23] L. M. Robeson, *J. Membr. Sci.* **1991**, *62*, 165.
[24] L. M. Robeson, *J. Membr. Sci.* **2008**, *320*, 390.
[25] M. Carta, M. Croad, R. Malpass-Evans, J. C. Jansen, P. Bernardo, G. Clarizia, K. Friess, M. Lanč, N. B. McKeown, *Adv. Mater.* **2014**, *26*, 3526.
[26] J. K. Adewole, A. L. Ahmad, S. Ismail, C. P. Leo, *Int. J. Greenhouse Gas Control* **2013**, *17*, 46.
[27] N. Du, M. M. Dal-Cin, G. P. Robertson, M. D. Guiver, *Macromolecules* **2012**, *45*, 5134.
[28] W. Qiu, C. C. Chen, L. Xu, L. Cui, D. R. Paul, W. J. Koros, *Macromolecules* **2011**, *44*, 6046.
[29] A. M. Kratochvil, W. J. Koros, *Macromolecules* **2008**, *41*, 7920.
[30] R. Swaidan, B. Ghanem, E. Litwiller, I. Pinnau, *Macromolecules* **2015**, *48*, 6553.
[31] P. Bernardo, F. Bazzarelli, F. Tasselli, G. Clarizia, C. R. Mason, L. Maynard-Atem, P. M. Budd, M. Lanč, K. Pilnáček, O. Vopička, K. Friess, D. Fritsch, Y. P. Yampolskii, V. Shantarovich, J. C. Jansen, *Polymer* **2017**, *113*, 283.
[32] M. Carta, R. Malpass-Evans, M. Croad, Y. Rogan, J. C. Jansen, P. Bernardo, F. Bazzarelli, N. B. McKeown, *Science* **2013**, *339*, 303.
[33] Y. Huang, D. R. Paul, *Polymer* **2004**, *45*, 8377.
[34] J. H. Kim, W. J. Koros, D. R. Paul, *Polymer* **2006**, *47*, 3094.
[35] H. Lin, *Curr. Opin. Chem. Eng.* **2014**, *4*, 54.

